Design and Implementation of Electromagnetic Active Control Actuators

Mingsian R. Bai and Kwuen-Yieng Ou

Journal of Vibration and Control 2003 9: 997
DOI: 10.1177/10775463030098006

Design and Implementation of Electromagnetic Active Control Actuators

MINGSIAN R. BAI
KWUEN-YIENG OU
Department of Mechanical Engineering, National Chiao-Tung University, 1001 Ta-Hsueh Road, Hsin-Chu 300, Taiwan, Republic of China

(Received 10 December 2001; accepted 8 July 2002)

Abstract: We present the modeling, parameter identification and design procedure of a linear voice-coil motor. A numerical simulation has been carried out to facilitate system integration. In particular, we use electromechanical analogy and the time-domain identification procedure with the eigensystem realization algorithm to predict the system response. In order to evaluate the performance of the voice-coil motor, we conducted an experimental investigation. Voice-coil motors mounted on a ball bearing housing are used for generating counter forces to cancel the transverse vibrations of a shaft. A controller is designed by using generalized predictive control. Multiple channel active control systems are implemented on the platform of a digital signal processor. Numerical and experimental results indicated that the designed actuators were effective in suppressing the periodic disturbances in rotors.

Key Words: voice-coil motor, eigensystem realization algorithm, vibrations, generalized predictive control

1. INTRODUCTION

In recent years, the development of active vibration control devices for rotating machinery in the industry has received much attention. Palazzolo et al. (1991) developed an active system using "piezoelectric pushers" for suppressing the steady and transient states of rotor vibration. Schweitzer (1985) and Ulbricht and Anton (1984) examined the stability and observability of rotor bearing systems with active vibration control. Their analysis related force and stiffness to electrical and geometrical properties of the electromagnetic bearings. Nikolajsen et al. (1979) examined the application of magnetic dampers to a 3.2 m simulated marine propulsion system. Heinzmann et al. (1980) employed loudspeaker coils linked to the shaft via ball bearings to control vibrations. Previously, in Bai and Lou (2000), we have presented some test results and adaptive control scheme for electromagnetic actuator based active vibration control. The electromagnetic actuator has several potential advantages for the generation of forces or motions when compared to hydraulic, pneumatic, or mechanical devices. It is possible to have very low friction, and the control of current through power electronics can be achieved rapidly and reliably so that force levels can be readily controlled. In contrast to competitive actuator types, the electromagnetic actuator is inherently linear which can be an advantage.

Journal of Vibration and Control, **9:** 997–1017, 2003 DOI: 10.1177/107754603030574

In this paper, we discuss the electromagnetic actuator modeling, parameter identification using the eigensystem realization algorithm (ERA) (Juang, 1994) and design. First, we mention the prototype of the optimal linear electromagnetic actuator that can be applied in the rotor system. The proposed actuator operates primarily by means of electromagnetic interactions between a voice coil and a permanent magnet. The device is purposed to produce linear motions with large forces that are required in active rotor vibration control. A Nd–Fe–B cylindrical magnet is used to generate high-flux-density magnetic field. Another Nd–Fe–B disk magnet is used to generate an anti-field such that the flux leakage is minimized. Two ring-shaped flex suspensions are employed for accurate alignment. To ease maintenance, the key components are designed to be detachable. The configuration of the device is optimized with the smallest physical size and weight to produce maximal response. On the other hand, the simulation of the actuator performance can be evaluated by modeling with electromagnetic analogy and parameter identification with the ERA. It is worth mentioning that the simulation result is the guideline of the optimization of the actuator design. In order to reach the desired performance, we should adjust the physical properties of the key components according to the simulation result. Finally, the test results corresponding to incorporating linear voice-coil motors (LVCMs) as actuator devices for active vibration control of the rotor system. An active technique for suppressing rotor vibration is proposed. Voice-coil motors mounted on a ball-bearing housing are employed to generate the required counter forces for active control. The control method employed in this paper is generalized predictive control (GPC); see Clarke and Mohtadi (1989) and Clarke et al. (1987). LVCMs were designed to serve as the actuators in the active control system. The numerical simulation and experimental investigations indicate that the proposed method and actuators are effective in suppressing the transverse vibrations in both horizontal and vertical directions to the shaft.

2. ELECTROMECHANICAL MODELING OF THE LVCM

A lumped-parameter model of a LVCM has been developed to describe actuator behavior for purposes of control system analysis and design, and, in particular, for certain applications requiring accurate position and/or force control. In the following, an analysis of the LVCM is presented by using electromechanical analogy. This subject is the application of electrical-circuit theory to the solution of mechanical and acoustical problems. This paper is focused on the design and analysis of the actuator with loading. It is reasonable to ignore the acoustical impedance. The resulting equivalent circuit is shown in Figure 1(a), where mobility analogy is used on the mechanical side. Although the equivalent circuit in Figure 1(a) is in the form of graphic language, it is entirely based on Newton's second law, Lorentz force and Kirchhoff's circuit laws. The details of how this circuit is derived are tedious but standard in the literature – see, for example, Beranek (1996) – and thus omitted for brevity. The analysis is limited to the low-frequency region where the voice coil acts as a piston and the enclosure is active in controlling the behavior of the LVCM. First, the symbols are defined. e_g is the open-circuit voltage (volts) of the generator. R_g is the resistance (ohms) of the generator. R_E is the resistance of the voice coil. L_E is the inductance of the voice coil,

$$L_E = \frac{N^2 \mu_0 A_C}{\ell_C}, \tag{1}$$

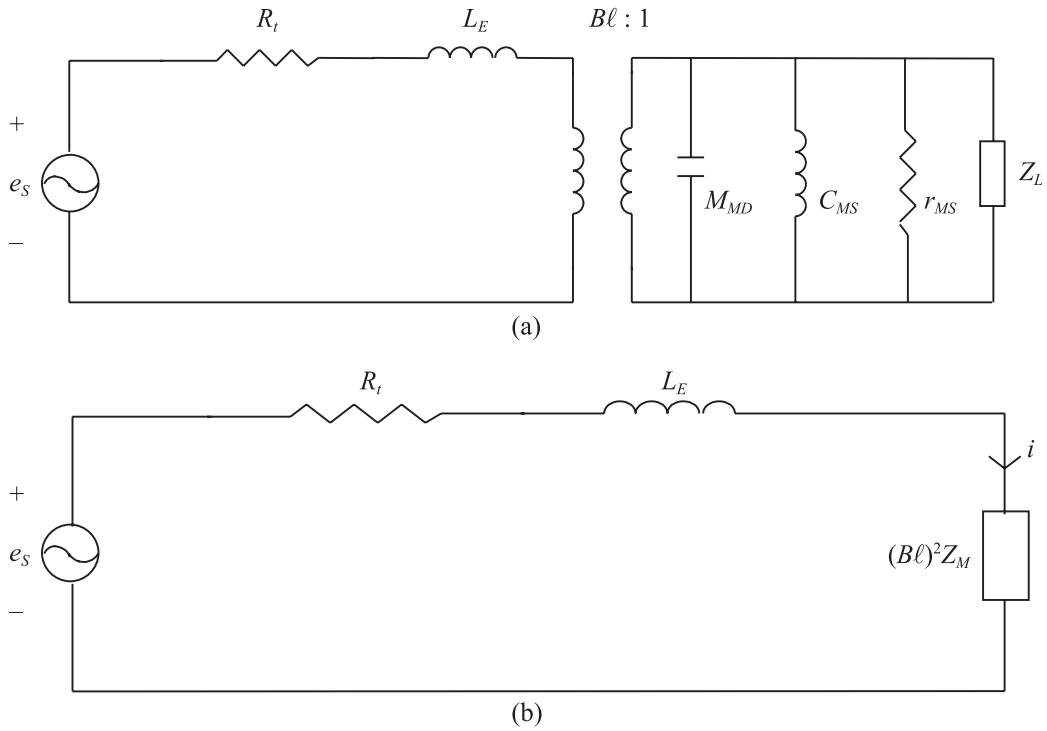

Figure 1. Electromechanical analysis of the LVCM. (a) The mobility analogy circuit of the LVCM; (b) the circuit of the mechanical side brought through the transformer to the electrical side.

where A_C is the cross area of the coil, ℓ_C is the total length of the coil, N is the number of turns of the coil and $\mu_0 = 4\pi \times 10^{-7}$. B is the steady air-gap flux density in webers per square meter. ℓ is the wire length in meters on the voice-coil winding. e is the voltage (volts) through the voice-coil winding. i is the electric current (ampere) through the voice-coil winding. u_c is the voice-coil velocity (meters per second). f_c is the force (newtons) generated by interaction between the alternating and steady states. M_{MD} is the mass of the piston and the voice coil in kilograms. r_{MS} is the mechanical responsiveness (meters per newton-second). R_{MS} is the reciprocal of r_{MS}. C_{MS} is the total mechanical compliance (meters per newton) of the suspension. z_L is the mechanical loading mobility (mks mechanical mohms). Z_L is the reciprocal of z_L.

The circuit of Figure 1(a) with the mechanical side brought through the transformer to the electrical side is shown in Figure 1(b). The equivalent mechanical mobility is

$$z_M = (1/j\omega M_{MD}) \| r_{MS} \| j\omega C_{MS} \| z_L,$$

where "$\|$" represents parallel connection. It is not difficult to show

$$\frac{i}{e_g} = \frac{1}{R_t + j\omega L_E + (B\ell)^2 z_M}, \tag{2}$$

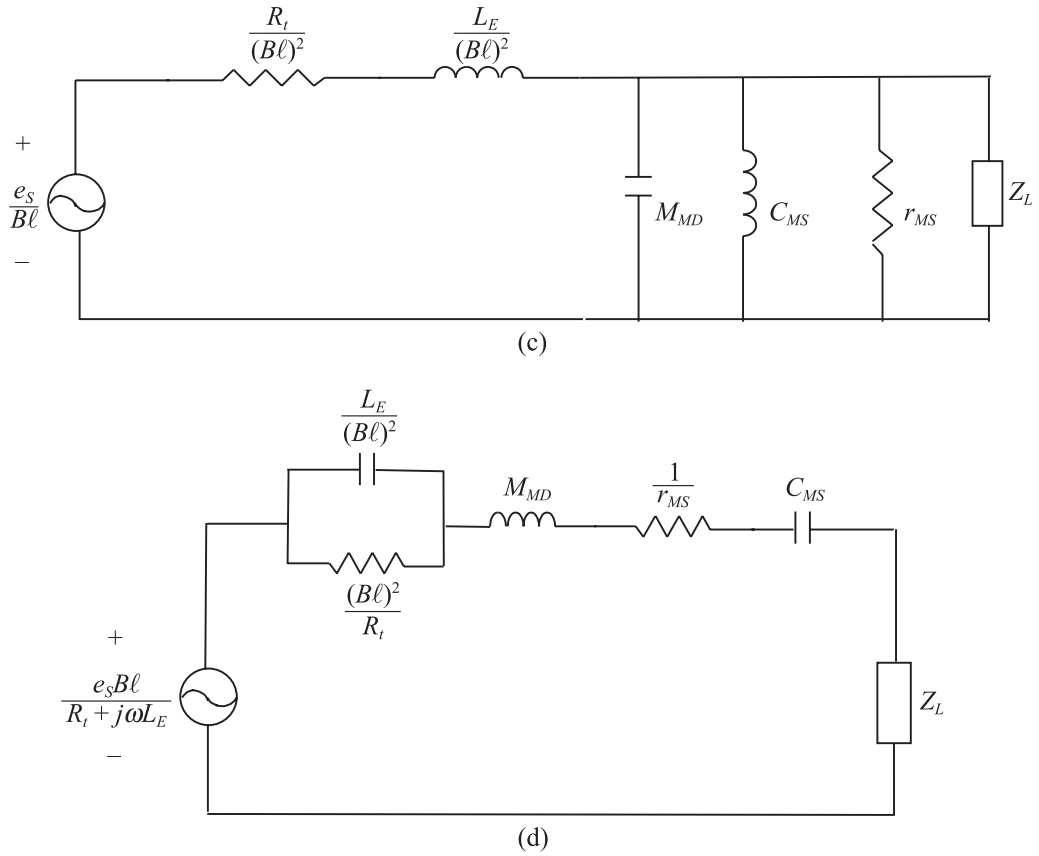

Figure 1. Electromechanical analysis of the LVCM. (c) the circuit of the electrical side brought through the transformer to the mechanical side; (d) the equivalent impedance analogy circuit of (c).

$$\frac{i}{e_g} = \frac{(j\omega)^2 M_{MD} + j\omega r_{MS} + 1/C_{MS}}{(j\omega)^3 L_E M_{MD} + (j\omega)^2 [R_t M_{MD} + L_E r_{MS}] + j\omega \left[\frac{L_E}{C_{MS}} + R_t r_{MS} + B^2\ell^2 \right] + \frac{R_t}{C_{MS}}} \tag{3}$$

where $R_t = R_g + R_E$.

In low frequency, $|j\omega L_E| << R_t$

$$\frac{i}{e_g} \cong \frac{(j\omega)^2 M_{MD} + j\omega r_{MS} + 1/C_{MS}}{(j\omega)^2 R_t M_{MD} + j\omega (R_t + B^2\ell^2) + R_t/C_{MS}}. \tag{4}$$

The frequency-dependent LVCM impedance is the reciprocal of Equation (4). Thus, in low frequency, the LVCM behaves as a second-order system with the resonance frequency:

$$\omega_n = \sqrt{\frac{1}{M_{MD}\, C_{MS}}}. \tag{5}$$

The circuit of Figure 1(a) with the electrical side brought through the transformer to the mechanical side is shown in Figure 1(c). It can be transformed into the impedance analogy equivalent circuit, as shown in Figure 1(d). According to Figure 1(d), the blocked force f_S, source impedance reflected to the mechanical side Z_S and free velocity V_0 are derived as follows,

$$f_S = \frac{e_S B\ell}{R_t + j\omega L_E} \tag{6}$$

$$\begin{aligned} N_Z &= (j\omega)^3 M_{MD}\, C_{MS}\, L_E + (j\omega)^2 [M_{MD}\, C_{MS}\, R_t + C_{MS}\, L_E R_{MS}\,] \\ &+ (j\omega)\left[C_{MS}\, R_{MS}\, R_t + (B\ell)^2 C_{MS} + L_E\right] + R_t, \\ D_Z &= (j\omega)^2 C_{MS}\, L_E + (j\omega)\, C_{MS}\, R_t, \\ Z_S &= \frac{N_Z}{D_Z} \end{aligned} \tag{7}$$

where R_{MS} is the reciprocal of the r_{MS}.

Similarly, in low frequency, $|j\omega L_E| \ll R_t$

$$Z_S = \frac{(j\omega)^2 M_{MD}\, C_{MS}\, R_t + (j\omega)\, C_{MS}\, R_{MS}\, R_t + (B\ell)^2 C_{MS} + R_t}{(j\omega)\, C_{MS}\, R_t} \tag{8}$$

Consequently, it is simple to obtain the frequency response of free velocity V_0 with the following equation:

$$V_0 = f_S Z_S. \tag{9}$$

3. PARAMETER IDENTIFICATION AND DESIGN PROCEDURES

In this paper, the LVCM is designed as the actuator to generate control force for vibration suppression. The efficient design and parameter identification procedures are developed. In accordance with the parameter measurement and the model simulation, the components of the LVCM are adjusted to achieve the desired performance. An LVCM is schematically shown in Figure 3. A rare-earth Nd–Fe–B cylindrical magnet is used to generate high intensity magnetic field. The configuration of the device is optimized with minimal physical size and weight to produce maximal response.

3.1. Parameter Identification

The parameters of the LVCM are identified by the following procedures:

(1) Measure the impedance curve and perform curve fitting of coefficients of the following transfer function:

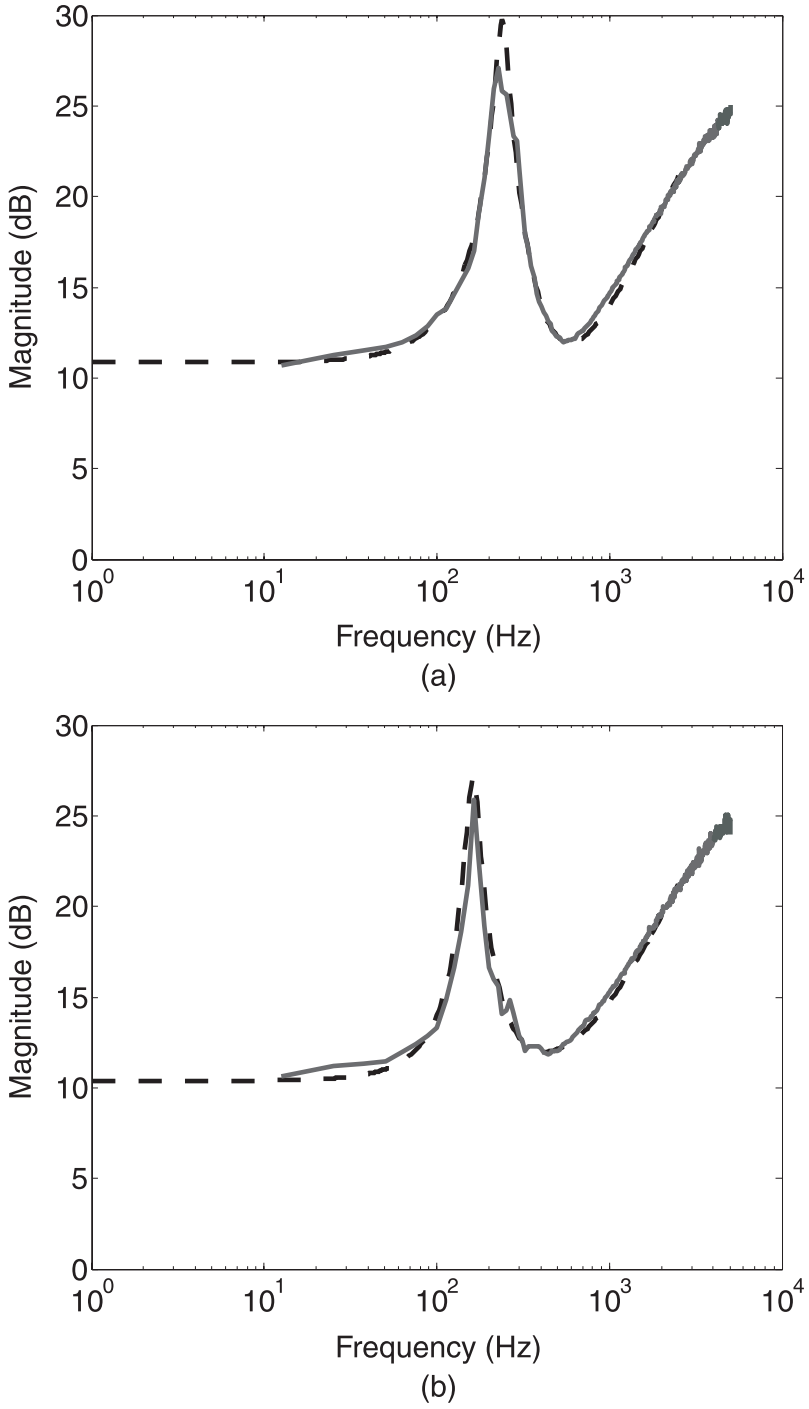

Figure 2. Impedance curves of the LVCM: (a) "free" LVCM; (b) "loaded" LVCM (— measured; -- regenerated).

$$
\begin{aligned}
N(s) &= s^3 L_E + s^2 \left(R_t + \frac{L_E}{R_{MS}\, M_{MD}} \right) \\
&\quad + s \left(\frac{L_E}{C_{MS}\, M_{MD}} + \frac{R_t}{R_{MS}\, M_{MD}} + \frac{B^2 \ell^2}{M_{MD}} \right) + \frac{R_t}{M_{MD}\, C_{MS}}, \\
D(s) &= s^2 + \frac{s}{R_{MS}\, M_{MD}} + \frac{1}{M_{MD}\, C_{MS}}, \\
Z(s) &= \frac{N(s)}{D(s)}, \qquad (10)
\end{aligned}
$$

where Equation (10) is identical to the reciprocal of Equation (3) and $s = j\omega$ is the Lapalace transform variable, In this paper, curve fitting is performed by using the ERA which is introduced in the next section. The result is shown in Figure 2(a).

(2) Add a mass of known weight (M_1) and repeat step 1 to obtain a new resonant frequency ω_2, as shown in Figure 2(b). Hence,

$$\omega_1 = \frac{1}{\sqrt{M_{MD}\, C_{MS}}} \qquad (11)$$

$$\omega_2 = \frac{1}{\sqrt{(M_{MD} + M_1)\, C_{MS}}}. \qquad (12)$$

From Equations (11) and (12), we obtain

$$M_{MD} = \frac{M_1}{\left(\frac{\omega_1}{\omega_2} \right)^2 - 1} \qquad (13)$$

$$C_{MS} = \frac{1}{M_1} \left(\frac{1}{\omega_2^2} - \frac{1}{\omega_1^2} \right). \qquad (14)$$

(3) Perform curve fitting of coefficients of the measured impedance curve of the LVCM. From the known coefficients in step 2 and comparing with the derived transfer function, we can extract all the necessary parameters including R_t, R_{MS} , L_E and the motor constant $B\ell$.

(4) Based on the obtained parameters, the frequency response of the LVCM including the blocked force, free velocity and the source impedance reflected to the mechanical side can be evaluated by Equations (6), (7) and (9).

3.2. Design Procedures

The desired efficacy of the LVCM is intended for large force generation, linear motion in wider frequency band, accurate alignment, and small physical size and weight. In order to

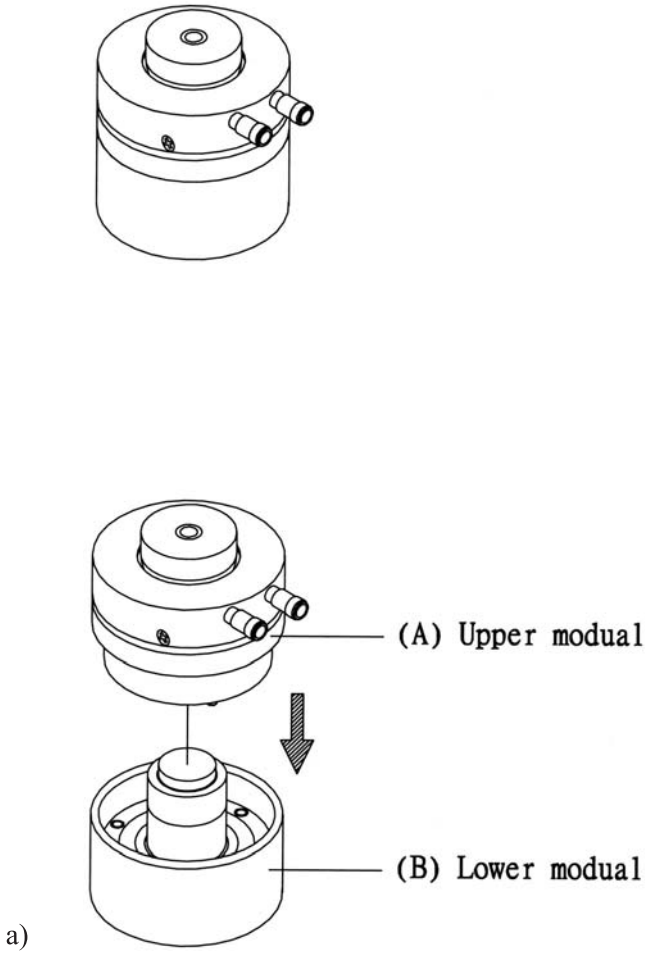

Figure 3. The design of the voice-coil motor: (a) outer appearance.

realize these statements, the design procedures of the LVCM are developed and outlined as follows.

(1) Choose a large $B\ell$ constant for ensuring sufficient output level. It is preferable to achieve this by using a strong magnet rather than increasing the length of the coil, because the latter approach has an adverse effect of increasing resistance and inductance. In this case, a Nd–Fe–B cylindrical magnet is used to generate high-flux-density magnetic field to guarantee a large $B\ell$ constant.
(2) Flux leakage in the enclosure causes the energy loss of the actuator operation and reduces the generated force and efficiency. In order to minimize the flux leakage, another disc magnet is used to generate the anti-field to raise the flux-density magnetic field.
(3) Choose the suitable material to manufacture the suspension based on the specific application. In general, the softer suspension has better performance in low frequency but may cause alignment inaccuracy. On the other hand, the harder suspension has better

b)

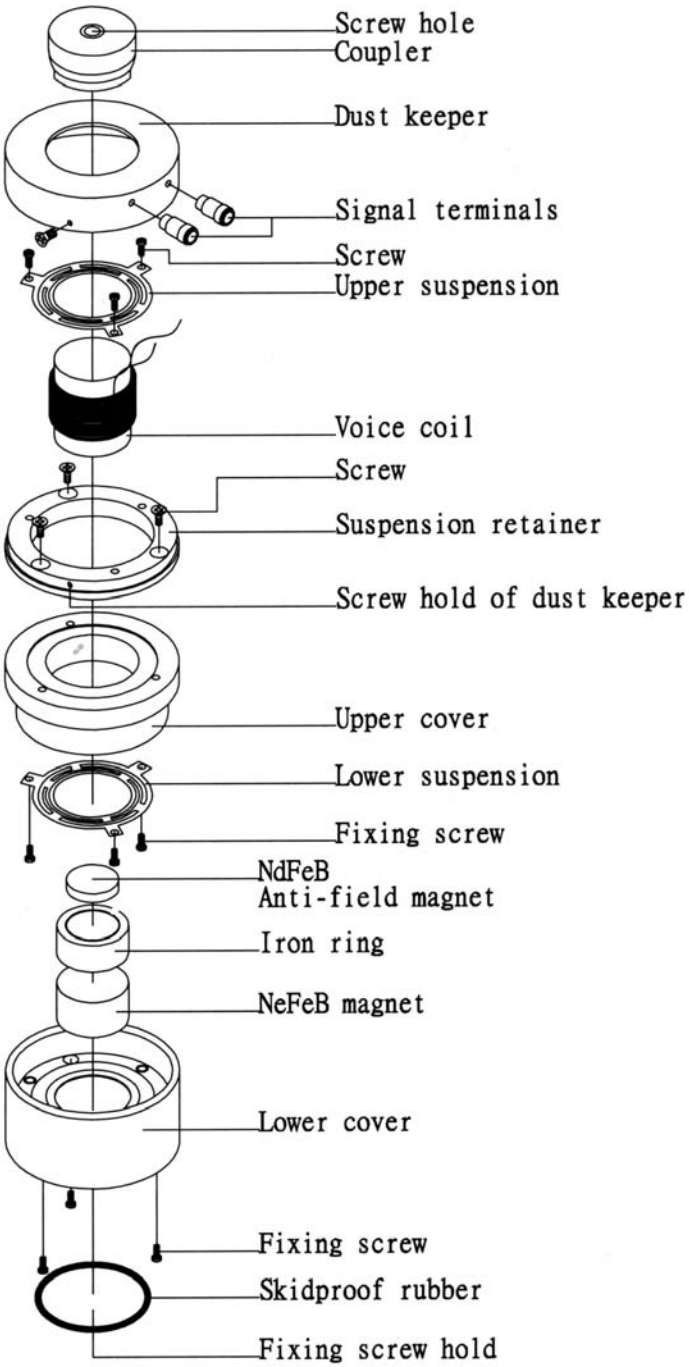

Figure 3 continued. The design of the voice-coil motor: (b) detailed structure.

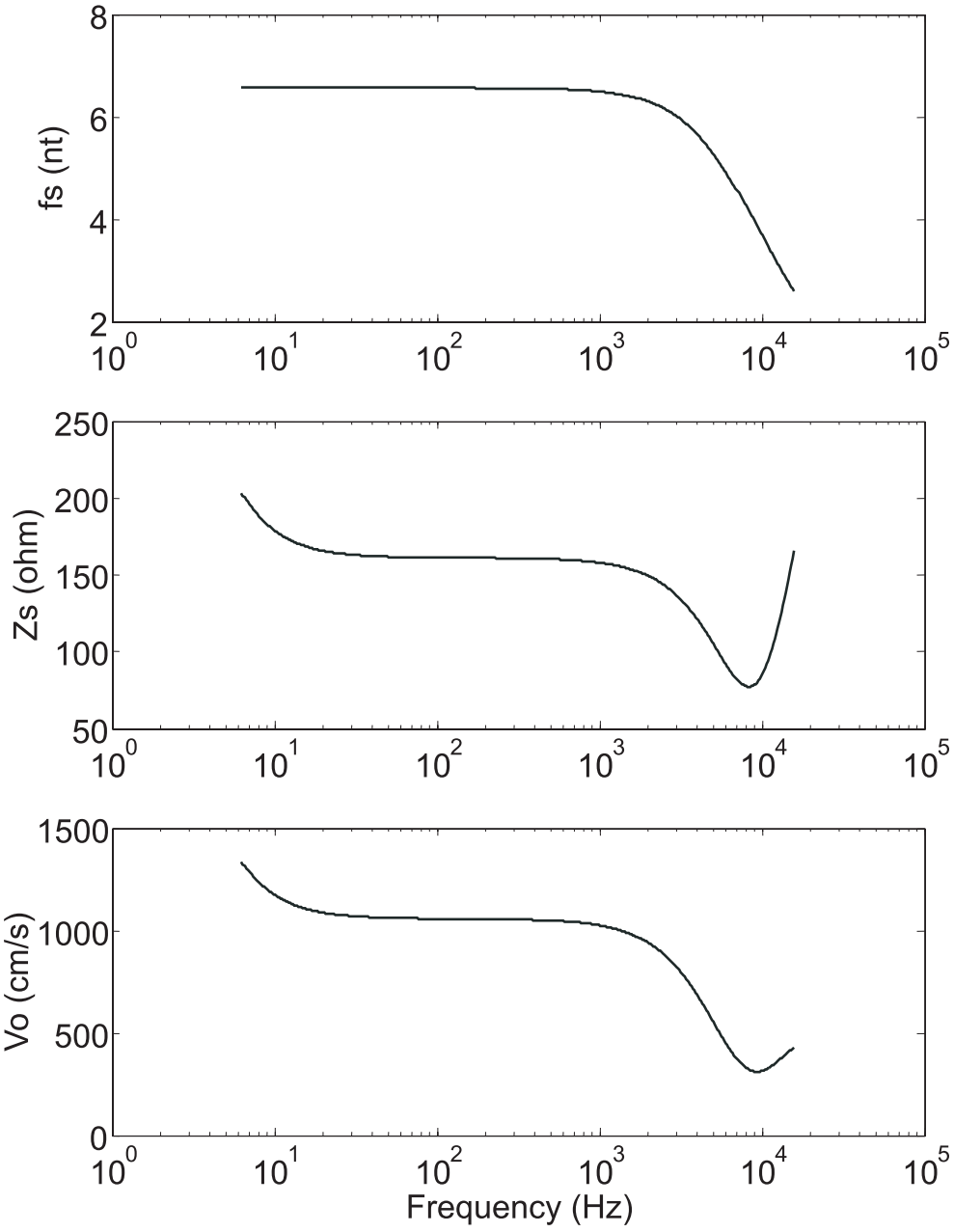

Figure 4. The LVCM response includes of the force generation, mechanical impedance, and free velocity.

performance in high frequency but causes smaller amplitude of the vibration. In this paper, based on the consideration of accurate alignment and working frequency, two ring flex suspensions are employed.

(4) According to the conception of the previous steps, make an embryo of the LVCM. Then, execute the parameter identification procedure to obtain all coefficients of aforementioned impedance model. Use these known parameters to simulate the frequency response of the blocked force, source impedance reflected to the mechanical side, and the free velocity of the LVCM.

(5) Verify the resemblance between simulation and desired performance, and regulate the parameters to attain the requirement by computer estimation. It is important that the value change of the parameters in simulation is related to the variety of the component properties of the LCVM. According to the simulation result, it is reliable to adjust the component properties of the LCVM to reach the desired performance. Thus, from the model simulation, we can obtain an idea of the performance of the LVCM before it is practically implemented.

Following the proposed design procedure and parameter obtaining method, the suitable LVCM can be designed efficiently. In this work, the LVCM is made following the proposed scheme and the performance is shown in Figure 4.

4. EIGENSYSTEM REALIZATION ALGORITHM

The identification method employed in this paper is the ERA (Juang, 1994). The state-space representation of a linear discrete-time system is

$$\mathbf{x}(k+1) = \mathbf{A}\mathbf{x}(k) + \mathbf{B}\mathbf{u}(k) \tag{15}$$

$$\mathbf{y}(k) = \mathbf{C}\mathbf{x}(k) + \mathbf{D}\mathbf{u}(k) \tag{16}$$

where k is the time step, $\mathbf{x}(k)$ is an $n \times 1$ state vector, $\mathbf{u}(k)$ is an $r \times 1$ input vector, and $\mathbf{y}(k)$ is an $m \times 1$ output vector. Consider the pulse-response matrix $\mathbf{Y}_k$ with dimensions $m \times r$ as follows:

$$\mathbf{Y}_0 = \mathbf{D}, \quad \mathbf{Y}_1 = \mathbf{CB}, \quad \mathbf{Y}_2 = \mathbf{CAB}, \quad \ldots\ldots, \quad \mathbf{Y}_k = \mathbf{CA}^{k-1}\mathbf{B}. \tag{17}$$

The $\alpha m \times \beta r$ Hankel matrix $\mathbf{H}(k-1)$ is composed of Markov parameters from Equation (17).

$$\mathbf{H}(k-1) = \begin{bmatrix} Y_k & Y_{k+1} & \cdots & Y_{k+\beta-1} \\ Y_{k+1} & Y_{k+2} & \cdots & Y_{k+\beta} \\ \vdots & \vdots & \ddots & \vdots \\ Y_{k+\alpha-1} & Y_{k+\alpha} & \cdots & Y_{k+\alpha+\beta-1} \end{bmatrix}. \tag{18}$$

If $\alpha \geq n$, $\beta \geq n$, and n is the order of the system, the matrix $\mathbf{H}(k-1)$ is of rank n. Substituting Markov parameters from Equation (17) into Equation (18) and decomposing $\mathbf{H}(k-1)$ into three matrices yield

$$\mathbf{H}(k-1) = \mathbf{P}_\alpha \mathbf{A}^{k-1} \mathbf{Q}_\beta. \tag{19}$$

The block matrix $\mathbf{P}_\alpha$ is the observability matrix and the matrix $\mathbf{Q}_\beta$ is the controllability matrix. If the system is controllable and observable, the block matrices $\mathbf{P}_\alpha$ and $\mathbf{Q}_\beta$ are both rank of n. Therefore, the Hankel matrix is of rank n by Equation (18).

Assume that there exists a matrix $\mathbf{H}^+$ satisfying both relations,

$$\mathbf{Q}_\beta \mathbf{H}^+ \mathbf{P}_\alpha = \mathbf{I}_n \tag{20}$$

$$\mathbf{H}(0)\,\mathbf{H}^+\mathbf{H}(0) = \mathbf{P}_\alpha \mathbf{Q}_\beta \mathbf{H}^+ \mathbf{P}_\alpha \mathbf{Q}_\beta = \mathbf{P}_\alpha \mathbf{Q}_\beta = \mathbf{H}(0). \tag{21}$$

Therefore, the matrix $\mathbf{H}^+$ is the pseudo-inverse of the matrix $\mathbf{H}(0)$. Perform singular value decomposition (SVD) on the matrix $\mathbf{H}(0)$,

$$\mathbf{H}(0) = \mathbf{R}\ \mathbf{\Sigma}\mathbf{S}^{\mathrm{T}} \tag{22}$$

where the columns of matrices $\mathbf{R}$ and $\mathbf{S}$ are orthonormal and $\mathbf{\Sigma}$ is a rectangular matrix

$$\mathbf{\Sigma} = \begin{bmatrix} \mathbf{\Sigma}_n & 0 \\ 0 & 0 \end{bmatrix} \tag{23}$$

with $\mathbf{\Sigma}_n = \mathrm{diag}\,[\sigma_1, \sigma_2, \cdots, \sigma_i, \sigma_{i+1}, \cdots, \sigma_n]$ and monotonically non-increasing. It should be mentioned that SVD is a mathematically general decomposition which is not restricted to any particular type of physical problem. On the other hand, it is numerically stable and "regularization" can often be carried out by replacing exceedingly small singular values by zeros.

Let $\mathbf{R}_n$ and $\mathbf{S}_n$ be the matrices formed by first n columns of $\mathbf{R}$ and $\mathbf{S}$. Hence, the matrix $\mathbf{H}(0)$ and its pseudo-inverse becomes

$$\mathbf{H}(0) = \mathbf{R}_n \mathbf{\Sigma}\mathbf{S}_n^{\mathrm{T}} \quad \text{where } R_n^{\mathrm{T}}\mathbf{R}_n = \mathbf{I}_n = \mathbf{S}_n^{\mathrm{T}}\mathbf{S}_n \tag{24}$$

and

$$\mathbf{H}^+ = \mathbf{S}_n \mathbf{\Sigma}_n^{-1}\mathbf{R}_n^{\mathrm{T}}. \tag{25}$$

In order to make both $\mathbf{P}_\alpha$ and $\mathbf{Q}_\beta$ balance, choose $\mathbf{P}_\alpha = \mathbf{R}_n \mathbf{\Sigma}_n^{1/2}$ and $\mathbf{Q}_\beta = \mathbf{\Sigma}_n^{1/2}\mathbf{S}_n^{\mathrm{T}}$. Substituting $k = 2$ in Equation (19) leads to Equation (26):

$$\mathbf{H}(1) = \mathbf{P}_\alpha \mathbf{A}\mathbf{Q}_\beta = \mathbf{R}\mathbf{\Sigma}_n^{1/2}\mathbf{A}\mathbf{\Sigma}_n^{1/2}\mathbf{S}_n^{\mathrm{T}}. \tag{26}$$

One obvious solution for the state matrix $\mathbf{A}$ is shown as follows:

$$\mathbf{A} = \mathbf{\Sigma}_n^{-1/2}\mathbf{R}_n^{\mathrm{T}}\mathbf{H}(1)\,\mathbf{S}_n\,\mathbf{\Sigma}_n^{-1/2}. \tag{27}$$

Using Equations (19), (20), (24) and (26), a minimum order realization can be obtained as follows:

$$\mathbf{Y}_k = \mathbf{E}_m^{\mathrm{T}}\mathbf{R}_n\mathbf{\Sigma}_n^{1/2}\left[\mathbf{\Sigma}_n^{-1/2}\mathbf{R}_n^{\mathrm{T}}\mathbf{H}(1)\,\mathbf{S}_n\,\mathbf{\Sigma}_n^{-1/2}\right]^{k-1}\mathbf{\Sigma}_n^{1/2}\mathbf{S}_n^{\mathrm{T}}\mathbf{E}_r. \tag{28}$$

This is the basic formulation of realization for the ERA. The estimated system is a minimum realization system and the system matrices are shown as

$$\hat{\mathbf{A}} = \boldsymbol{\Sigma}_n^{-1/2}\mathbf{R}_n^{\mathrm{T}}\mathbf{H}(1)\,\mathbf{S}_n\,\boldsymbol{\Sigma}_n^{-1/2}, \quad \hat{\mathbf{B}} = \boldsymbol{\Sigma}_n^{1/2}\mathbf{S}_n^{\mathrm{T}}\mathbf{E}_r, \quad \hat{\mathbf{C}} = \mathbf{E}_m^{\mathrm{T}}\mathbf{R}_n\,\boldsymbol{\Sigma}_n^{1/2}, \quad \hat{\mathbf{D}} = \mathbf{Y}_0. \tag{29}$$

Finally, transfer $\hat{\mathbf{A}}$, $\hat{\mathbf{B}}$, $\hat{\mathbf{C}}$, $\hat{\mathbf{D}}$ to an identified discrete-time model in modal coordinates

$$\begin{aligned} x_m\,(k+1) &= \hat{\boldsymbol{\Lambda}}x_m\,(k) + \hat{\mathbf{B}}_m\,u\,(k) \\ y\,(k) &= \hat{\mathbf{C}}_m\,x_m\,(k) + \hat{\mathbf{D}}u\,(k) \end{aligned} \tag{30}$$

where $\hat{\boldsymbol{\Lambda}} = \mathrm{diag}\,(\hat{\lambda}_1, \hat{\lambda}_2, \cdots, \hat{\lambda}_n)$, $\hat{\mathbf{B}}_m = [\hat{b}_1^{\mathrm{T}}\ \ \hat{b}_2^{\mathrm{T}}\ \ \cdots\ \ \hat{b}_n^{\mathrm{T}}]$, $\hat{\mathbf{C}}_m = [\hat{c}_1\ \ \hat{c}_2\ \ \cdots\ \ \hat{c}_n]$ $\hat{\lambda}_i (i = 1, 2, \ldots, n)$ are the eigenvalues of the $\hat{\boldsymbol{\Lambda}}$ matrix, where n is the number of modal coordinates.

The computational steps of the ERA are summarized as follows:

1. Construct a block of Hankel matrix $\mathbf{H}(0)$ by arranging the Markov parameters (pulse response samples) into blocks with α, β selected.
2. Decompose $\mathbf{H}(0)$ with singular value decomposition.
3. Determine the order of the system by examining the singular values of the Hankel matrix $\mathbf{H}(0)$.
4. Construct a minimum order realization $\hat{\mathbf{A}}$, $\hat{\mathbf{B}}$, $\hat{\mathbf{C}}$, $\hat{\mathbf{D}}$ using a shifted block Hankel matrix $\mathbf{H}(1)$.
5. Find the eigensolution of the realized state matrix and transform the realized model to modal coordinates.

5. APPLICATION EXAMPLE: ACTIVE BEARING FOR ROTORS

5.1. Experimental Investigation

A rotor simulator was constructed to serve this purpose. Referring to Figures 6(a) and (b), the system consists of a 1130 g aluminum disc (6.6 cm in diameter) mounted on a shaft (50 cm in length and 2 cm in diameter) which is driven at the right end by a three-phase, 220 V, two-hp induction motor. The motor speed can be controlled with an inverter. There are 16 equally spaced threaded holes drilled on the disc at which we can mount a mass (three 4 g bolts) to create imbalance. The rotor is supported by two ball bearings. Two designed linear voice-coil motors are mounted on the horizontal and vertical directions at the left-end bearing housing. A resin column is used at the vertical support to improve mechanical stability and robustness. The actuators are connected to the output of a DSP, TMS320C32, in conjunction with a four-input/four-output I/O module. Two eddy current sensors mounted near the disc for measuring the shaft displacements are connected to the input of the DSP. A photo switch is used to generate pulses from a reflector on the disc. The rotating speed is then determined by a frequency counting algorithm (Kuo and Morgan, 1996). This completes a DSP-based active vibration control system for the rotor.

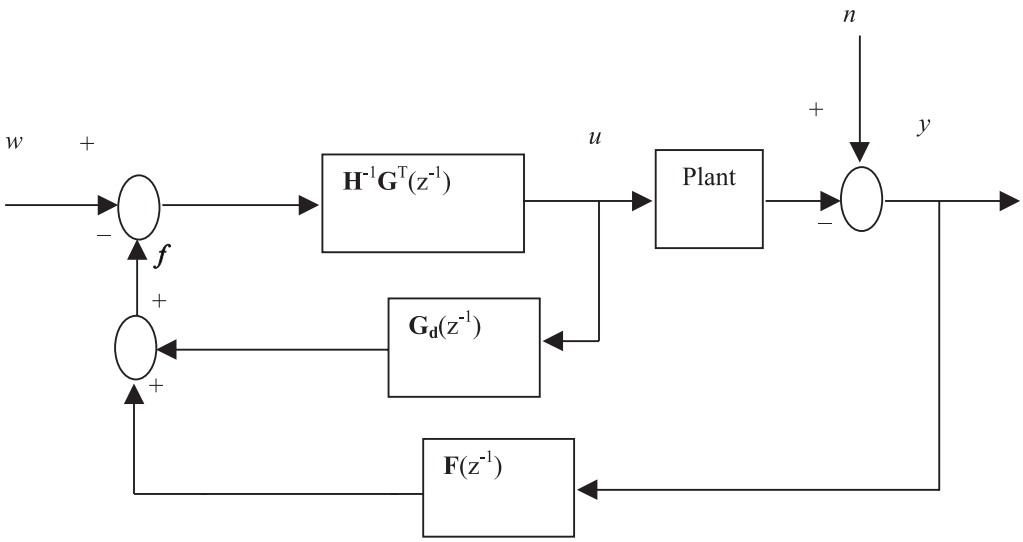

Figure 5. The block diagram of the general predictive control.

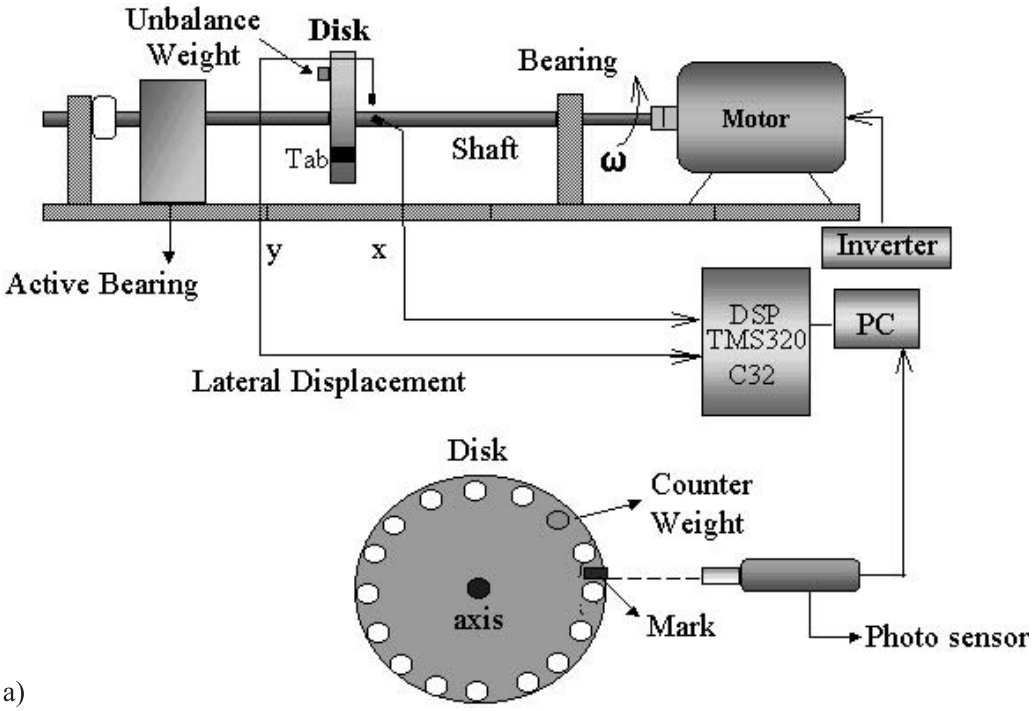

a)

Figure 6. The experimental arrangement of the rotor-bearing system: (a) side view.

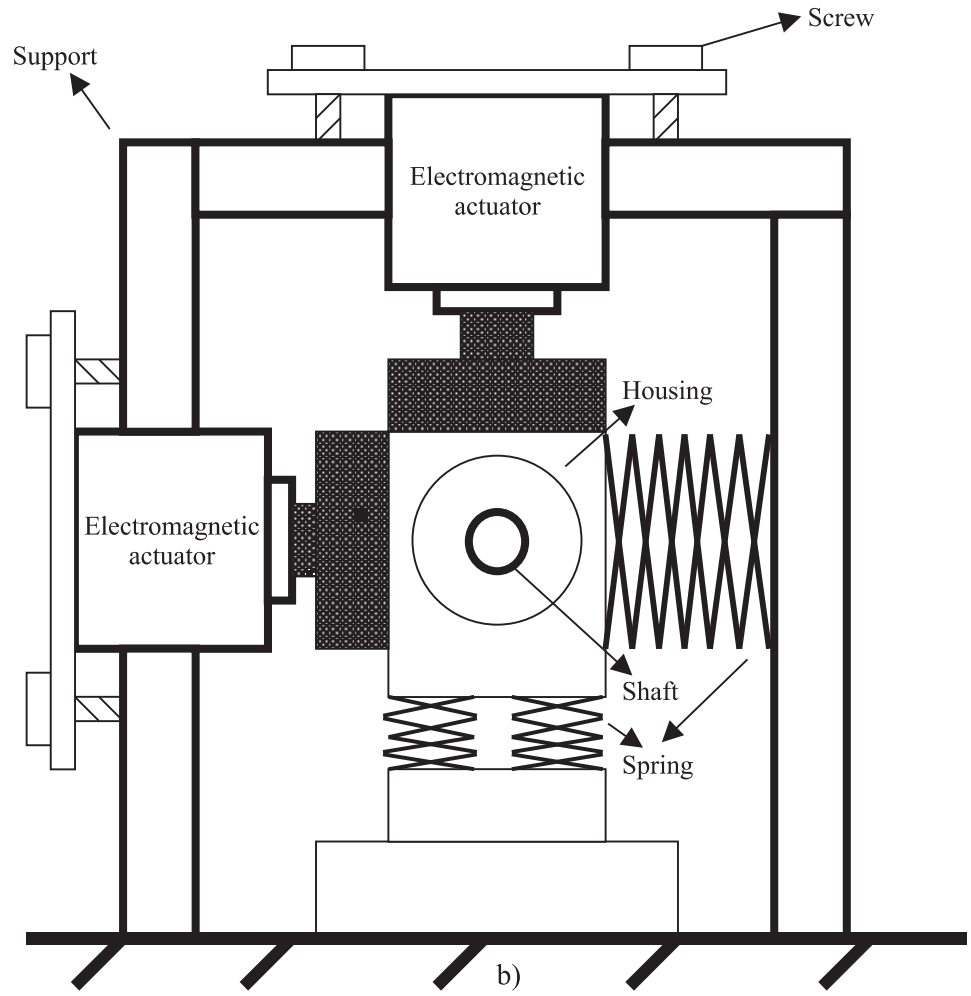

Figure 6 *continued*. The experimental arrangement of the rotor-bearing system: (b) axial view.

Prior to controller design, the two-input/two-output system model is established by using the ERA. The control bandwidth is therefore selected as 10–100 Hz, where the modeling error and the higher-order dynamics of the plant do not present problems for the narrow-band control.

5.2. Control Algorithm

The general idea of GPC is given in the following (Clarke and Mohtadi, 1989; Clarke et al., 1987). A linear time-invariant system can be described by an auto-regressive moving-average model,

$$A\left(z^{-1}\right) y\left(t\right) = z^{-d} B\left(z^{-1}\right) u\left(t-1\right) + \frac{e\left(t\right)}{\Delta}, \tag{31}$$

where $u(t)$ and $y(t)$ are the control and output of the plant, $e(t)$ is a zero mean white noise, and d is the dead time of the system. Because the goal in our problem is to reject the harmonic disturbances generated by the rotor, an internal model $\Delta = 1 - 2\cos(\omega_0)\zeta z^{-1} + \zeta z^{-2}$ is utilized for rejection of a pure-tone vibration at the rotating frequency ω_0 of the shaft, where ζ is damping ratio. This approach differs from conventional applications, where a model for "set-point" reference is generally adopted. Thus the optimal prediction of $y(t+j)$ is

$$\widehat{y}\langle t+j \mid t\rangle = G_j\left(z^{-1}\right)\Delta u\left(t+j-d-1\right) + F_j\left(z^{-1}\right)y\left(t\right). \tag{32}$$

The polynomial G_{j+1} can be calculated recursively:

$$G_{j+1} = E_{j+1}\,\mathrm{B}. \tag{33}$$

The coefficients of F_{j+1} and E_{j+1} can be found by solving the Diophantine equation:

$$T\left(z^{-1}\right) = E_j\left(z^{-1}\right)\Delta A\left(z^{-1}\right) + z^{-j}F_j\left(z^{-1}\right). \tag{34}$$

T can be chosen such that $1/T$ is low pass. The terms dependent on past data can be grouped into $\mathbf{f}$, which leads to

$$\mathbf{y} = \mathbf{G}\mathbf{u}_+ + \mathbf{f}. \tag{35}$$

In GPC, we seek to minimize the cost function J

$$J = \left(\mathbf{G}\mathbf{u}_+ + \mathbf{f} - \mathbf{w}\right)^{\mathrm{T}}\left(\mathbf{G}\mathbf{u}_+ + \mathbf{f} - \mathbf{w}\right) + \lambda\,\mathbf{u}_+^{\mathrm{T}}\mathbf{u}_+. \tag{36}$$

Prediction horizons are chosen to N and define the following matrices

$$\mathbf{w} = \left[w\left(t+d+1\right) \quad w\left(t+d+2\right) \quad \cdots \quad w\left(t+d+N\right)\right]^{\mathrm{T}} \tag{37}$$

$$\mathbf{H} = 2\left(\mathbf{G}^{\mathrm{T}}\mathbf{G} + \lambda\mathbf{I}\right) \tag{38}$$

$$\mathbf{b}^{\mathrm{T}} = 2\left(\mathbf{f} - \mathbf{w}\right)^{\mathrm{T}}\mathbf{G} \tag{39}$$

where $\mathbf{w}$ is the reference signal. Although the problem in the work is essentially a noise rejection problem, we reformulate the problem into a tracking problem as in most literature on GPC. In this regard, the reference signal is selected to be a signal coherent to the periodic disturbances, with much smaller (but not zero) amplitude. A tachometer signal is required to generate the reference with fundamental frequency and its multiples. Minimization of J then leads to the control law

$$\mathbf{u} = -\mathbf{H}^{-1}\mathbf{b}. \tag{40}$$

The block diagram of GPC is shown in Figure 5. $\mathbf{H}$ is the *Toeplitz* matrix whose inverse multiple by $\mathbf{G}^{\mathrm{T}}$ can be found by the Levinson–Durbin algorithm (Papamichalis, 1987). In GPC, only the first element of $\mathbf{u}$ is retained and the rest of data are discarded.

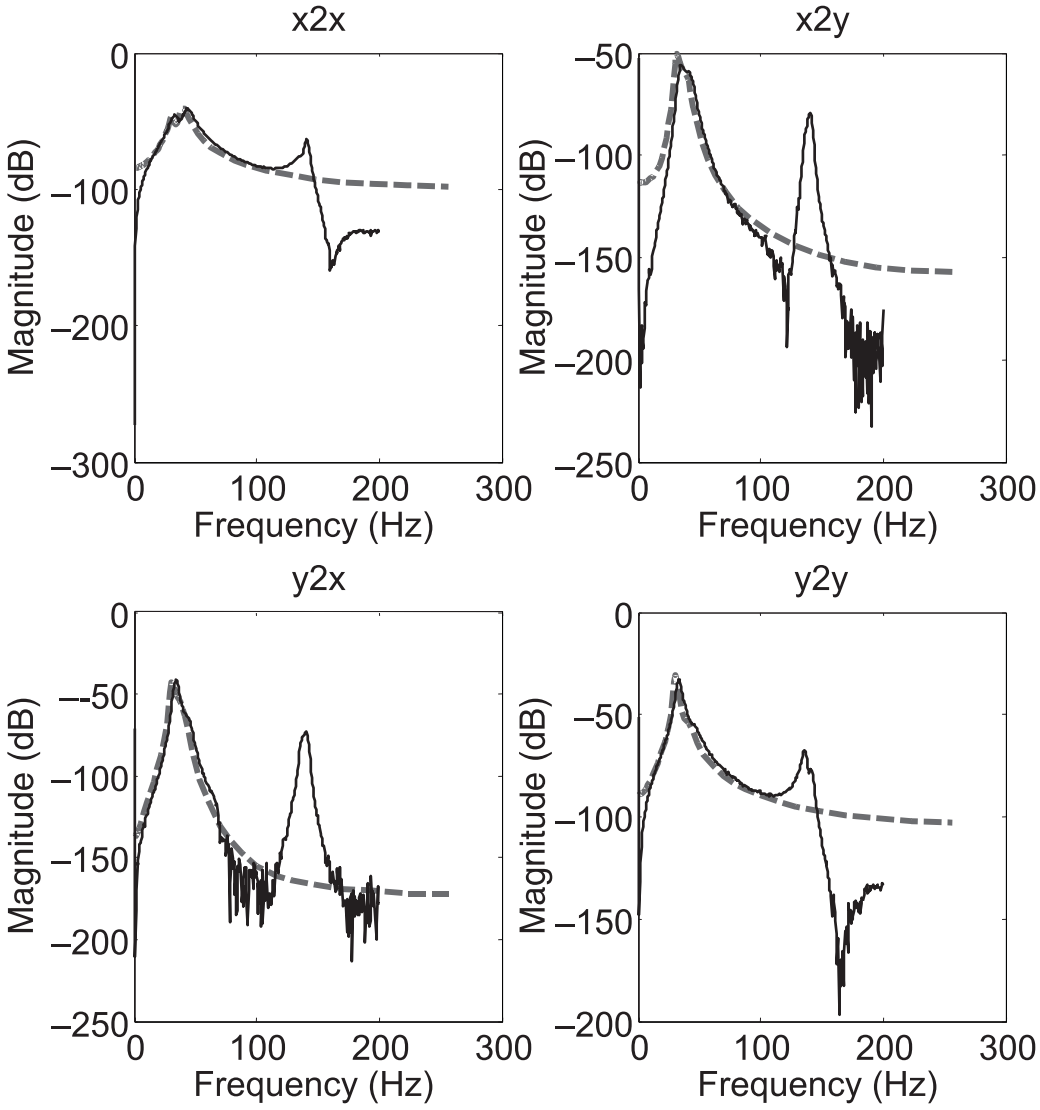

Figure 7. Frequency response of the active bearing system: — measured; - - regenerated.

5.3. Experimental Result

The transfer function obtained using the system identification procedure is compared with the measured frequency response in Figure 7. The identified transfer function is a six-order bi-proper function. The sampling rate is 2 kHz and the rotor speed is 50 Hz. In the GPC synthesis, the predictive horizon is set to be 3, $T(z^{-1}) = 1 - p \cdot z^{-1}$, where p is chosen to be the pole of the plant transfer function farthest to the origin, $\lambda = 0.8$, $\zeta = 0.995$, ω_0 is estimated by frequency counting of the photo switch signal, and reference signal $w(k) = 0.001 \sin(\omega_0 k)$. The dead time $d = 2$, due to the two-sample delay in

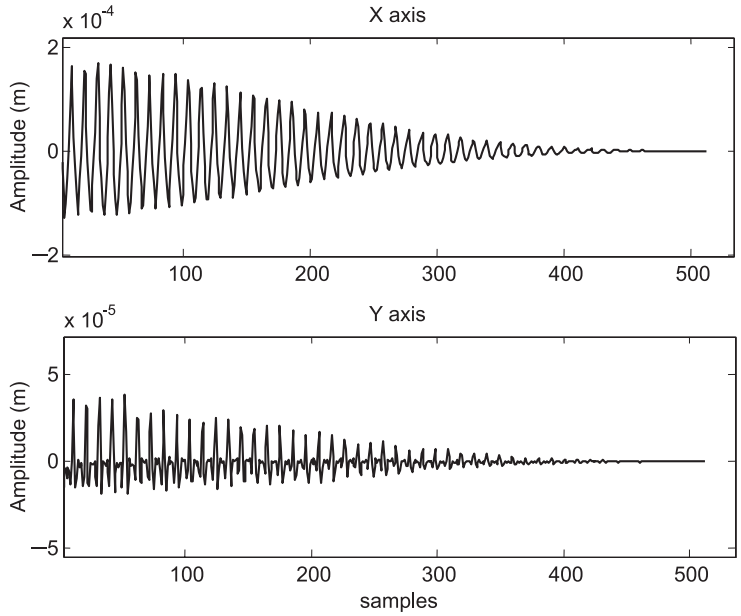

Figure 8. Time histories of shaft displacement of general predictive control experiment result with a speed of 50 Hz.

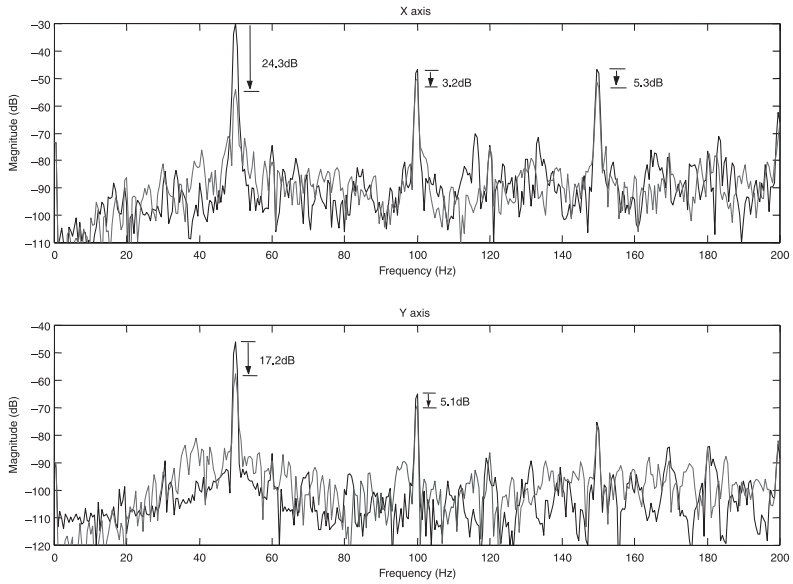

Figure 9. Power spectrum of shaft displacement of general predictive control experiment result with a speed of 50 Hz: — original system; - - controlled system.

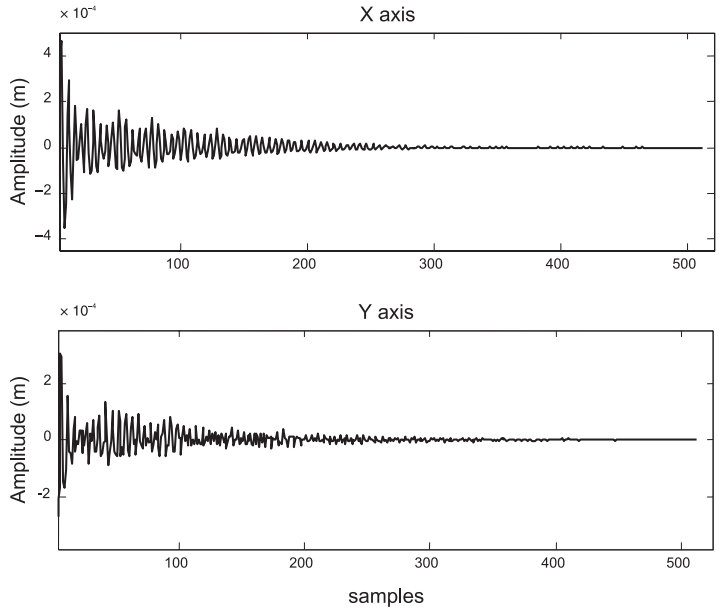

Figure 10. Time histories of shaft displacement of general predictive control experiment result with a speed of 40–50 Hz.

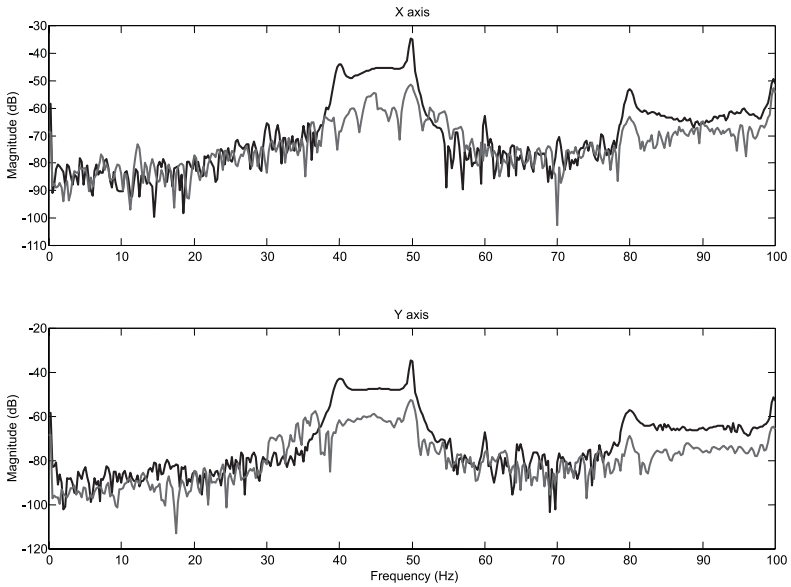

Figure 11. Power spectrum of shaft displacement of general predictive control experiment result with a speed of 40–50 Hz: — original system; - - controlled system.

AD/DA conversion. The matrix $\mathbf{H}^{-1}\mathbf{G}^{\mathrm{T}}$ is adapted during each sampling period by using the Levinson–Durbin algorithm. It can be observed from the test result in Figures 8 and 9 that maximum attenuations obtained at the *X*-axis and *Y*-axis reach 24.3 dB and 17.2 dB at 50 Hz, respectively. Furthermore, the rotor speed is varied from 40 to 50 Hz with a slew rate 10 Hz s^{-1}. The experimental result is shown in the time domain (Figure 10) and the frequency domain (Figure 11). It is shown that, even for a varying speed with fast slew rate, appreciable attenuation (approximately 20 dB in the band 40–50 Hz) can still be achieved. The factors that contribute to the effectiveness of the proposed control system are summarized as follows. First, the actuator of the control system is based on the proposed procedure in the revised paper. It guarantees the achievement of the optimal response in the desired control bandwidth. Secondly, a second-order internal model of the GPC algorithm, $\Delta = 1 - 2\cos(\omega_0)\zeta z^{-1} + \zeta z^{-2}$, is utilized for rejection of a harmonic disturbance at the rotating frequency ω_0 of the shaft. Thirdly, on-line and real-time parameter estimation is incorporated to the GPC algorithms to cope with system uncertainties and perturbations.

6. CONCLUSIONS

In this paper, we have analyzed the lumped model of the LVCM in terms of the mechanical impedance, force generation, and free velocity. Although this may be sufficient for the present study, a more sophisticated modeling approach dealing with the frequency-dependent mechanical impedance, force generation, and free velocity are presented to improve the accuracy of the response prediction. Simulation tools were developed to facilitate system integration and design procedures were also summarized. By performing the curve fitting with the ERA and comparing the coefficients between the identified result and analytic model, all the LVCM parameters will be attained. Furthermore, the LVCM behavior can be simulated immediately. The major advantage of the proposed simulation tool is that it can predict the LVCM response without multifarious measurement and calculation. It is simple and efficient in contrast to other methods published in the literature. In designing the actuator, a prototype must be constructed first. After evaluating the proposed measure scheme, we adjust the parameter value to achieve the desired response with simulation tools provided in the paper. According to the value change of each parameter in the simulation, we replace the suitable components to complete the realization. It is obvious that the design procedures developed in the paper are more efficient than traditional design methods such as trial and error. On the other hand, an experiment is executed to test the performance of the designed actuator. The GPC algorithm was implemented using two linear voice-coil motors affixed to the bearing housing. Experimental investigation indicates that the scheme combining the designed LVCM and the GPC algorithm is effective in attenuating periodic vibrations in the rotor. The proposed scheme is able to reject the vibrations of not only fixed speed rotors but also varying speed rotors.

Acknowledgments. This work was supported by the National Science Council in Taiwan, Republic of China, under the project number NSC 89-2212-E009-007. We would also like to thank also Dr. Gary H. Koopmann, Center of Acoustics and Vibration at Penn State University for the motivation for this research topic.

REFERENCES

Bai, M. R. and Lou, W., 2000, "DSP implementation of an active bearing mount for rotors using hybrid control," *ASME Journal of Vibrations and Acoustics* **122**, 420–428.

Beranek, L. L., 1996, *Acoustics*, Acoustical Society of America, Woodbury, NY.

Clarke, D. W. and Mohtadi, C., 1989, "Properties of generalized predictive control," *Automatica*, **25**, 859–875.

Clarke, D. W., Mohtadi, C., and Tuffs, P. S., 1987, "Generalized predictive control-part I. The basic algorithm," *Automatica*, **23**, 137–148.

Heinzmann, J., et al., 1980, "The implementation of automatic vibration control in a high speed rotating test facility," *University of Virginia Report* UVA/464761/MAE80/160.

Juang, J. N., 1994, *Applied System Identification*, Prentice Hall, Englewood Cliffs, NJ.

Kuo, S. M. and Morgan, D. R., 1996, *Active Noise Control Systems*, Wiley, New York.

Nikolajsen, J., Holmes, R., and Gondholekar, V., 1979, "Investigation of an electromagnetic damper for vibration control of a transmission shaft," *Proceedings of the Institution of Mechanical Engineers* **193**, 331–336.

Palazzolo, A. B., et al., 1991, "Test and Theory for Piezoelectric Actuator-Active Vibration Control of Rotating Machinery," *ASME Journal of Vibrations and Acoustics* **113**, 167–175.

Papamichalis, P. E., 1987, *Practical Approaches to Speech Coding*, Prentice Hall, Englewood Cliffs, NJ.

Schweitzer, G., 1985, *Magnetic Bearings for Vibration Control*, Bently Nevada Instability Seminar, Minden, NV.

Ulbricht, H. and Anton, E., 1984, "Theory and application of magnetic bearing with integrated displacement and velocity sensors," in *I. Mech. E, Conference on Rotordynamics*, Paper C299/84.